

The Journal of Immunology

This information is current as
of June 9, 2010

**Chronic Rejection Triggers the
Development of an Aggressive
Intra-graft Immune Response through
Recapitulation of Lymphoid
Organogenesis**

Olivier Thaunat, Natacha Patey, Giuseppina Caligiuri,
Chantal Gautreau, Maria Mamani-Matsuda, Yahia Mekki,
Marie-Caroline Dieu-Nosjean, Gérard Eberl, René
Ecochard, Jean-Baptiste Michel, Stéphanie Graff-Dubois
and Antonino Nicoletti

J. Immunol. published online Jun 4, 2010;
doi:10.4049/jimmunol.0903589

Subscriptions

Information about subscribing to *The Journal of Immunology* is
online at <http://www.jimmunol.org/subscriptions/>

Permissions

Submit copyright permission requests at
<http://www.aai.org/ji/copyright.html>

Email Alerts

Receive free email alerts when new articles cite this article. Sign
up at <http://www.jimmunol.org/subscriptions/etoc.shtml>

Chronic Rejection Triggers the Development of an Aggressive Intragraft Immune Response through Recapitulation of Lymphoid Organogenesis

Olivier Thauat,^{*,†,‡,§,¶} Natacha Patey,^{||} Giuseppina Caligiuri,^{*,#} Chantal Gautreau,^{**,†} Maria Mamani-Matsuda,^{††} Yahia Mekki,^{‡‡} Marie-Caroline Dieu-Nosjean,^{*,†,§§} Gérard Eberl,^{¶¶} René Ecochard,^{|||} Jean-Baptiste Michel,[#] Stéphanie Graff-Dubois,^{*,†,#,1} and Antonino Nicoletti^{*,†,#,1}

The unwarranted persistence of the immunoinflammatory process turns this critical component of the body's natural defenses into a destructive mechanism, which is involved in a wide range of diseases, including chronic rejection. Performing a comprehensive analysis of human kidney grafts explanted because of terminal chronic rejection, we observed that the inflammatory infiltrate becomes organized into an ectopic lymphoid tissue, which harbors the maturation of a local humoral immune response. Interestingly, intragraft humoral immune response appeared uncoupled from the systemic response because the repertoires of locally produced and circulating alloantibodies only minimally overlapped. The organization of the immune effectors within adult human inflamed tissues recapitulates the biological program recently identified in murine embryos during the ontogeny of secondary lymphoid organs. When this recapitulation was incomplete, intragraft B cell maturation was impeded, limiting the aggressiveness of the local humoral response. Identification of the molecular checkpoints critical for completion of the lymphoid neogenesis program should help develop innovative therapeutic strategies to fight chronic inflammation. *The Journal of Immunology*, 2010, 185: 000–000.

The immunoinflammatory process aims at eliminating the target Ag. Stringent regulatory mechanisms normally ensure that this process is transient and is turned off when the causative stimulus has been cleared. Difficulty in eradicating Ags leads to sustained inflammation, which is responsible for extensive tissue destruction and loss of function.

The progression toward chronic inflammation is characterized by a gradual shift in the type of immune effectors present at the inflammation site, namely, an enrichment of cells from the adaptive immune system (1). In addition the organization of infiltrated cells is also modified. Indeed, it has long been observed that inflammatory cells can organize themselves into structures that morphologically resemble secondary lymphoid organ follicles (2). The process by which organized lymphoid structures ("tertiary lymphoid tissues") appear de novo during chronic inflammation has been referred to as lymphoid neogenesis (3, 4).

Seminal studies (5–7) have demonstrated that tertiary lymphoid tissues are permissive microenvironments for the induction of Ag-specific humoral immune responses and have led to the hypothesis that lymphoid neogenesis may contribute to the exacerbation of chronic inflammatory diseases. This process has therefore received increasing attention, and the list of diseases in which tertiary lymphoid tissue has been observed is growing longer (8).

Chronic rejection provides optimal conditions to study the immune mechanisms involved in the development of chronic inflammation-associated tertiary lymphoid tissues. Indeed, 1) tertiary lymphoid tissues have systematically been detected in chronically rejected grafts (9–12); 2) the Ags targeted by the immune system are known (recipient-mismatched HLA Ags of the transplanted tissues); 3) the mechanisms by which inflammation becomes chronic rely on the sustained replenishment of the Ag from the rejected tissue; and 4) chronically rejected

*Institut National de la Santé et de la Recherche Médicale U872, Centre de Recherche des Cordeliers; [†]Université Pierre et Marie Curie; [‡]Service d'Anatomopathologie, Hôpital Necker, Assistance Publique Hôpitaux de Paris; [§]Institut National de la Santé et de la Recherche Médicale U698, Centre Hospitalier de l'Université Xavier Bichat; [¶]Laboratoire d'Immunologie et d'Histocompatibilité, Hôpital Saint-Louis, Assistance Publique Hôpitaux de Paris; ^{||}Institut National de la Santé et de la Recherche Médicale U783, Développement du Système Immunitaire, Université Paris Descartes, Faculté de Médecine, Site Necker-Enfants Malades; ^{|||}Université Paris Descartes, Unité Mixte de Recherche S872; ^{††}Laboratoire du Développement du Tissu Lymphoïde, Centre National de la Recherche Scientifique URA1961, Institut Pasteur, Paris; ^{‡‡}Hospices Civils de Lyon, Hôpital Edouard Herriot, Service de Transplantation Rénale et d'Immunologie Clinique; ^{§§}Université de Lyon; ^{¶¶}Institut National de la Santé et de la Recherche Médicale U851; [#]Laboratoire de Virologie Est, Hôpital Femme Mère Enfant, Centre Hospitalier de l'Université-Hospices Civils de Lyon; and ¹Service de Biostatistique Santé, Unité Mixte de Recherche, Centre National de la Recherche Scientifique 5558, Université Claude Bernard Lyon I, Lyon Cedex 03, France

¹S.G.-D. and A.N. contributed equally to this work.

Received for publication November 6, 2009. Accepted for publication May 1, 2010.

This work was supported by grants from the Institut National de la Santé et de la Recherche Médicale, the Fondation pour la Recherche Médicale, the Fondation du Rein, and the Fondation de France.

Address correspondence and reprint requests to Dr. Olivier Thauat, Service de Transplantation Rénale et d'Immunologie Clinique, Hôpital Edouard Herriot, 5 Place d'Arsonval, 69437 Lyon Cedex 03, France. E-mail address: olivier.thauatpastu@free.fr

Abbreviations used in this paper: ADPKD, autosomal dominant polycystic kidney disease; Afr, African; Alport Sd, Alport syndrome; ATG, antithymocyte globulin; Aza, azathioprine; C, cadaveric; Cort Nec, cortical necrosis; CS, corticosteroid; Csa, cyclosporine A; DTR, detransplanted graft; ECGN, extracapillary glomerulonephritis; eGC, ectopic germinal center; ESRF, end-stage renal failure; Evero, everolimus; FDC, follicular dendritic cells; FK506, tacrolimus; FSGS, focal segmental glomerulosclerosis; HSP, Henoch Schonlein purpura; HUS, hemolytic and uremic syndrome; IS regimen, immunosuppressive treatment; L, living; LT, lymphotoxin; MFI, mean fluorescence intensity; MGN, membranous glomerulopathy; MMF, mycophenolate mofetil; NAS, nephroangiosclerosis; No. AR, number of biopsy-proven episodes of acute rejection; No. CMV dis, number of symptomatic CMV disease episodes; NoK, normal kidney; OKT3, anti-gCD3 Abs; QRT-PCR, quantitative real-time PCR; Rank of Tr, rank of transplantation; Rec, recurrence; Siro, sirolimus; TMA, thrombotic microangiopathy.

Copyright © 2010 by The American Association of Immunologists, Inc. 0022-1767/10/\$16.00

organs are sometimes removed, providing a large amount of diseased tissue that can be comprehensively analyzed, at both the molecular and cellular levels.

In the current study, we show that in chronically rejected human kidneys, lymphoid neogenesis is analogous to the ontogenic program triggered in the embryo during the development of secondary lymphoid organs. The complete recapitulation of this program results in the generation of fully functional ectopic germinal centers (eGCs) that allows for the efficient maturation of a local humoral immune response, which hastens tissue destruction. In contrast, when this recapitulation was incomplete, local B cell maturation was impeded, limiting the aggressiveness of the intragraft humoral response.

Materials and Methods

Human samples

Renal allografts removed from 26 nonselected patients because of terminal failure were collected in four transplantation centers over a period of 3 y. The tissues were maintained in germ-free conditions at 4°C and were processed <24 h after explantation. The individual characteristics of these patients are presented in Table I.

The immunohistological analysis of the first eight explanted kidneys revealed that intragraft B cell nodules were phenotypically heterogeneous. The following 18 explanted grafts were therefore subjected to a more comprehensive analysis, which could not be applied retrospectively to detransplanted graft (DTR)1 to DTR8.

Fresh normal renal tissue was obtained from the intact portion of six kidneys removed for renal cancer.

This study was approved by the Local Ethic Committee, and all the patients gave informed consent for the use of the samples for research purposes.

Histopathology

The renal cortex of fresh explanted allografts or control kidneys were dissected and embedded in paraffin, or snap-frozen immediately in OCT medium (Tissue-Tek, Agar Scientific, Stansted, Essex, U.K.) in liquid nitrogen.

Ten-micrometer-thick cryosections and 4- μ m-thick paraffin sections were used. Routine examination was performed after Masson's trichrome, H&E-safran, periodic acid Schiff, and silver staining.

Indirect immunoperoxidase staining was performed with the following primary Abs: rabbit anti-human CD3 ϵ (polyclonal, Abcam, Paris, France), mouse anti-human CD20 (clone L26, Dako, Trappes, France), mouse anti-human follicular dendritic cells (clone CNA.42, Dako), rat anti-human PNAd, (clone MECA 79, BD Pharmingen, San Diego, CA), rabbit anti-human podoplanin (polyclonal, Sigma-Aldrich, St. Louis, MO), mouse anti-human IgD (clone IA6-2, BD Pharmingen), rabbit anti-AID (polyclonal, Kind gift from A. Durandy, Necker, Paris), mouse anti-human Bcl-2 (clone 124, Dako), mouse anti-human Bcl-6 (clone PG-B6p, Dako), mouse anti-human CD208/DC-LAMP (clone 104.G4, Beckman Coulter, Fullerton, CA), and mouse anti-human-CD138 (clone B-A38, Serotec, Oxford, U.K.). The first primary Ab was applied, followed by incubation with the appropriate biotinylated secondary Abs and with streptavidin peroxidase and 3,3'-diaminobenzidine-tetrachloride (ChemMate detection Kit, Dako). Negative staining control experiments were performed by omitting the primary Ab. Slides were counterstained with H&E (Dako).

Numbers of primary follicle-like nodules and of eGCs were evaluated blindly by a trained pathologist (N. Patey) at 50 \times magnification on 10 sections from four distinct paraffin-embedded blocks using a semi-quantitative scale ranging from 0 (samples without follicle/eGC) to 3 (samples with >5 follicles/eGC per field).

Molecular biology

mRNA extraction and RT. Total RNA was isolated from two distinct renal cortex tissue fragments from each of the 26 explanted grafts and from six control kidneys using the RNeasy Mini Kit (Qiagen, Valencia, CA). cDNAs were generated from 1 μ g total RNA using SuperScript II reverse transcriptase (Invitrogen, San Diego, CA) and random decamers (ABgene, Epsom, U.K.).

Primer design. The gene-specific primer sets are provided in the Table II. All the primers were designed using Primer3 software and obtained from Eurogentec (Angers, France).

Real-time quantitative PCR. Quantitative real-time PCR (QRT-PCR) was performed on an ABI Prism 7300 sequence detection system (Applied Biosystems, Foster City, CA) in a total volume of 24 μ l, containing 4 μ l cDNA sample, 8 μ l diluted primer set, and 12 μ l SYBR Green Master Mix

(Qiagen). The thermal cycling was carried out by starting at 95°C for a 10 min hold, followed by 50 amplification cycles at 95°C for 15 s and at 60°C for 60 s. Dissociation curve analysis was performed at the end of 50 cycles to verify the identity of the PCR product. No signals were detected in no-template controls. Results are expressed as threshold cycle values corresponding to the cycle at which PCR enters the exponential phase and were normalized to the threshold cycle value obtained with GAPDH house-keeping gene amplification. For each gene and each cDNA preparation, the PCR reactions were run five times and the results were averaged.

Cell biology

Cell suspension preparation. The renal cortexes of fresh explanted grafts were cut with a sterile razor blade into \sim 0.125 mm³ fragments that were incubated in a solution of 1 mg/ml collagenase A and 0.1 mg/ml DNase I (Roche Diagnostic Systems, Somerville, NJ) for 1 h at 37°C. Cell suspensions were passed through a 70- μ m cell strainer, and mononuclear cells were separated over Ficoll-Paque Plus (GE Healthcare, Saclay, France).

Flow cytometry. Ten million cells were incubated with a fluorescent mAb mixture (BD Biosciences, San Jose, CA) specific for the following human cell surface markers: CD19 (AmCyan, clone SJ25C1), CD138 (allophycocyanin, clone MI15), IgD (FITC, clone IA6-2), CD38 (PE, clone HB7) from BD Pharmingen; CD27 (allophycocyanin-Alexa Fluor 750, clone 0323) from eBioscience (San Diego, CA). More than 1×10^6 events in the lymphoid FSC/SSC gate were acquired on an LSR II flow cytometer and analyzed with DIVA software (BD Biosciences).

ELISPOT. The quantification of IgG-producing plasmacells was performed by ELISPOT as previously described (13, 14). Briefly, mononuclear cells isolated from kidneys were plated in complete culture medium and cultured for 6 d at 37°C, in a 5% CO₂ atmosphere. Cultured cells were serially diluted in culture medium, in triplicate, before transfer to ELISPOT plates. Multiscreen 96-well filter plates (Millipore, Bedford, MA) were coated by incubation overnight at 4°C with 10 μ g/ml anti-human Ig polyvalent Ab (Caltag Laboratories, Burlingame, CA). After 6 h of incubation at 37°C, ELISPOT was performed with 1 μ g/ml biotinylated goat anti-human IgG Fc (Caltag Laboratories), followed by 5 μ g/ml HRP-conjugated avidin D (Vector Laboratories, Burlingame, CA) and developed using 3-amino-9-ethylcarbazole (Sigma-Aldrich).

Quantification of memory B cells was conducted according to the same protocol, except that the cells were stimulated with an optimized mix of polyclonal mitogens: 10 ng/ml PWM extract (PWM, batch 1303H, ICN; MP Biomedicals, Aurora, OH), a 1/10,000 dilution of fixed *Staphylococcus aureus*, Cowan extract (SAC; Sigma-Aldrich), and 6 μ g/ml fully phosphothioated CpG (ODN-2006, Prologo; Sigma-Aldrich) during the 6-d culture preceding the ELISPOT assay.

Analysis of local Ig production

Tissue culture. Tissue cultures were performed as previously described (11). Briefly, 24 randomly selected fragments (\sim 0.5 mm³) of the renal cortex of explanted allografts were washed three times and cultured in a 24-well plate in 1 ml RPMI 1640 medium (Cambrex, East Rutherford, NJ) supplemented with 100 U/ml penicillin/streptomycin and 25 μ g/ml Fungizone (Life Technologies, Rockville, MD). Culture supernatants were harvested after 5 d of culture and stored at -20°C until further analysis.

ELISA. The concentrations of IgG, IgA, and IgM in the supernatants were measured using standard ELISA. Human IgG subclasses were quantified using a Human IgG Subclass Profile ELISA Kit (Zymed Laboratories, San Francisco, CA). ELISA was performed at least twice on three different tissue-culture wells.

Luminex. Luminex assays were used to detect the presence of anti-HLA alloantibodies in the supernatants (LifeScreen, Tepeel Lifecodes, Stamford, CT) and subsequently, to determine their specificity (LABScreen single Ag HLA class I and class II detection tests, One A).

Statistical analysis

Significant differences between the four clusters of gene expression were seek for: donor age, donor sex, donor type (living versus cadaveric), donor CMV status, recipient age, cause of end-stage renal failure, time spent on dialysis, recipient CMV status, rank of transplantation, immunosuppressive therapy (administration or not of an induction therapy, and anticalcineurin-based versus mammalian target of rapamycin-inhibitor-based regimen), number of biopsy-proven acute rejection episodes, and number of CMV disease episodes. Kruskal-Wallis rank test was used for quantitative parameters and Fisher exact test for qualitative variables.

In an attempt to determine whether the differences in the functionality of lymphoid neogenesis observed between the four clusters of gene expression were statistically significant, we performed the following analysis. The

variables that explore the same biological process were grouped in four characteristics as follows: 1) local germinal center reaction (*AID* relative expression), 2) local B cell maturation (average rank [1–6] of IgD^{neg} CD38^{bright} germinal center B cells among CD19^{pos} cells, proportion of CD27^{pos} among CD19^{pos} infiltrating the graft, proportion of plasmacells infiltrating the graft), 3) local IgG production (concentration of total IgG in the supernatant of tissue cultures, three different tissue-culture wells), 4) local humoral alloimmune response (density, diversity, and intensity of the local anti-HLA Ab production). Values were then ranked and transformed in z-scores to correct them for non-normality and the trend was tested using a regression analysis for repeated measures.

Graft survival in the cluster of gene expression was compared using Wilcoxon test.

Results

Microarchitecture of the inflammatory infiltrate during chronic rejection

Over a period of 3 y, 26 explanted nonselected renal grafts were analyzed. The individual characteristics of these patients are presented in Table I. In contrast with kidneys removed due to immediate primary surgical failure ($n = 3$), or nonimmune failure (angiosarcoma, $n = 1$; or recurrence of the renal disease, $n = 2$), all the 20 chronically rejected renal grafts were infiltrated by immune effectors. The possibility that inflammatory infiltration was related to CMV-induced tubulointerstitial nephritis was ruled out for 25/26 samples by the negativity of CMV QRT-PCR (Table I).

In the vast majority of chronically rejected renal grafts (19/20), the interstitial chronic inflammatory infiltrate displayed a highly organized microarchitecture similar to that of secondary lymphoid tissues (Fig. 1A). In particular, B cells were packed into nodular structures evocative of B cell follicles. The phenotypic characterization of B lymphocytes revealed the heterogenous nature of these nodules, as already reported in the synovia of rheumatoid arthritis patients (15). Two types of nodules could be identified; nodules composed of a uniform CD20^{pos} B cell population expressing IgD and Bcl-2 (Fig. 1B, left panels) were similar to primary follicles; whereas nodules with a core of CD20^{pos}IgD^{neg}Bcl-2^{neg} B cells, highly expressing Bcl-6 that had pushed aside the CD20^{pos}IgD^{pos} Bcl-2^{pos} B cells (Fig. 1B, right panels), resembled secondary follicles, namely, germinal centers. The ratio between these two types of structures differed between samples, and the number of eGCs did not increase with the quantity of primary nodules.

eGC formation during chronic inflammation requires the expression of genes involved in lymphoid organogenesis

We reasoned that the development of eGC during chronic inflammation could follow the same biological program as that identified in the embryo during the ontogeny of secondary lymphoid organs. The expression levels of a selected set of genes (Table II), reported to play key roles in lymphoid organogenesis (16–22), were quantified by QRT-PCR in each tissue sample, and in six normal kidneys, all of which were devoid of inflammation. Data were processed by hierarchical clustering to identify samples sharing a similar pattern of expression. Normal kidneys were characterized by a low level of expression for all lymphoid organogenesis genes. Strikingly, this pattern was shared by the three grafts explanted due to primary surgical failure (DTR11, DTR12, and DTR20) as well as by the three grafts explanted due to nonimmune mediated failure (DTR2, DTR10, and DTR16). All these samples were grouped in the C1 cluster (Fig. 2A). In the 20 remaining chronically rejected grafts, the level of expression of lymphoid organogenesis genes was heterogeneous, and samples could be split into three clusters: C2, C3, and C4 (Fig. 2A). In contrast to the samples of the C1 cluster, those of the C2, C3, and C4 clusters all expressed a common core of genes (*CXCL13* and *CXCR4*), the expression of which was as-

sociated with the recruitment of B cells organized into primary follicles (Fig. 2B). C3 and C4 additionally expressed *CCL19*, *CCL21*, *CCR7*, *LT α* , *LT β* , and *CXCR5*. Finally, *CXCL12* and *LT β* R were expressed only in samples from the C4 cluster, this latter therefore grouping together the samples that expressed the complete set of lymphoid organogenesis genes. The expression of these additional genes in the C3 and C4 clusters correlated with the detection of eGC by immunohistochemical analysis (Fig. 2C). The conversion of primary into secondary follicles was more efficient in the C4 samples because the number of eGC was higher in the C4 than in the C3 samples (1 ± 0.71 versus 0.50 ± 0.62 ; Fig. 2C), despite the fact that they evolved from a reduced quantity of primary nodules (1.00 ± 0.41 versus 1.70 ± 1.03 ; Fig. 2B).

Germinal center reaction is characterized by the expression of activation-induced cytidine deaminase (AID), the key enzyme controlling class switch recombination and somatic hypermutations. In accordance with recently published data (12, 23), AID protein was not detectable in naive B cells forming the primary follicles, but was readily evidenced in eGC B cells (Fig. 2D). Because this enzyme is mandatory for the production of high-affinity Abs endowed with adequate effector functions, the gradual increase in AID expression observed from C1 to C4 (Student *t* test = 5.52; $p < 0.001$) indicates that this gene expression-based clusterization defines functional clusters with respect to the maturation of the local humoral immune response (Fig. 2E).

To identify the genes whose expression contributed the most to distribute the samples into the four clusters, we performed a principal component analysis on the realtime QRT-PCR dataset. This analysis revealed that *CXCL13*, *CCL21*, and *LT β* R were the genes with the largest eigenvalues. Whereas the dendrogram scale, which illustrates the way each sample enters its cluster (Fig. 2A, right dendrogram), suggested a greater level of similarity between C1 and C2 on one hand, and C3 and C4 on the other, the discrimination between samples belonging to the C2 and C3 clusters appeared difficult along the first two eigenvectors (canon 1 and 2; Fig. 2F), indicating that C2 and C3 are highly related.

Lack of completion of the biological program results in impeded local B cell maturation

The maturation of B cells was analyzed by flow cytometry according to the Bm1–Bm5 classification, which is based on the expression of CD38 and IgD (24). This classification allows for the identification of the successive cell development stages, from naive B cells to differentiated memory B cells.

The proportion of CD19^{pos} cells in the inflammatory infiltrate (Fig. 3A) was concordant with the histological quantification of primary nodules (Fig. 2B) and further documented the paucity of the B cells in the C1 cluster samples.

Regarding the maturation of B cells, a gradual increase in the proportion of Bm5 memory B cells and a symmetric reduction of Bm1/Bm2 naive B cells was observed from the C2 to C4 samples (Fig. 3B). In the samples of the C4 cluster, in which the complete set of lymphoid organogenesis genes was expressed, the B cell maturation program appeared to be proceeding toward the memory stage unhindered. In contrast, B cell maturation in the C3 cluster was blocked at the Bm2'/Bm3 δ 4 δ pregerminal stage, because a marked reduction in Bm3 and Bm4 germinal center B cells was observed (Fig. 3B). In the C2 cluster B cells maturation was impeded, resulting in naive B cells accumulation (Fig. 3B). Bm5 B cells proportion was only slightly reduced in the C2 cluster, suggesting that a direct recruitment of memory B cells from the periphery is also possible.

The Bm1–Bm5 classification has recently been challenged by the demonstration that some Bm1 cells express the CD27 memory

Table 1. Clinical characteristics of the population studied

Characteristics of the Donor				Characteristics of the Recipient				Transplantation					
Age (y)/Sex	Donor Type	Anti-CMV IgG	Age (y)/Gender/Ethnicity	Cause of ESRF	Time on Dialysis (d)	Anti-CMV IgG	Rank of Tr	IS Regimen	No. AR	No. CMV Dis	Cause of Graft Failure	Time to Explantation (d)	Cluster
DTR1	55/F	+	26/F/Arab	Unknown	915	+	1	CS, Aza, Csa	1	0	Chronic rejection	1281	C3
DTR2	74/M	-	66/M/Afr	FSGS	488	+	1	Anti-IL-2R, CS, MMF, Csa	0	0	Rec FSGS	1098	C1
DTR3	43/M	+	15/F/White	Lupus	1983	+	2	ATG, CS, MMF, FK506	1	1	Chronic rejection	1677	C3
DTR4	35/F	-	43/F/White	ECGN	5033	+	2	ATG, CS, Csa	0	0	Chronic rejection	4728	C3
DTR5	60/M	+	57/F/White	ADPKD	1159	+	1	ATG, CS, MMF, FK506	2	2	Chronic rejection	2562	C2
DTR6	49/M	+	28/F/White	Lupus	3569	+	1	Anti-IL-2R, CS, MMF, FK506	3	0	Chronic rejection	2044	C2
DTR7	68/F	+	61/M/Afr	NAS	732	+	1	CS, MMF, Siro	1	0	Chronic rejection	1952	C4
DTR8	79/F	+	46/M/White	MGN	1251	+	1	Anti-IL-2R, CS, MMF, Csa	2	0	Chronic rejection	732	C2
DTR9	35/M	-	24/M/White	Uropathy	1311	+	2	OKT3, CS, Aza, Csa	0	0	Chronic rejection	1959	C4
DTR10	62/M	+	56/M/White	NAS	1159	+	1	CS, MMF, FK506	0	0	Angiosarcoma	183	C1
DTR11	38/M	+	39/M/White	HSP	4240	+	2	Anti-IL-2R, CS, MMF, FK506	0	0	Arterial thrombosis	10	C1
DTR12	57/F	+	41/M/White	Unknown	3660	+	1	ATG, CS, MMF, FK506	0	0 ^a	Arterial thrombosis	6	C1
DTR13	18/M	-	40/F/White	Alport Sd	1586	-	1	CS, MMF, FK506	0	0	Chronic rejection	1647	C3
DTR14	17/M	-	22/M/White	FSGS	2135	-	1	ATG, CS, Aza, FK506	0	0	Chronic rejection	3721	C2
DTR15	46/F	+	40/F/Afr	TMA	579	+	1	Anti-CD7, CS, Aza, Csa	1	1	Chronic rejection	5917	C2
DTR16	59/M	+	24/M/Afr	Uropathy	702	+	1	Anti-IL-2R, CS, MMF, Csa	0	0	Rec TMA	671	C1
DTR17	55/M	+	27/F/White	Uropathy	422	+	1	CS, MMF, FK506	1	0	Chronic rejection	2644	C2
DTR18	16/F	-	7/M/Arab	HUS	1183	+	2	CS, Aza, Csa	1	0	Chronic rejection	6147	C3
DTR19	41/F	+	36/M/White	Berger	122	+	1	Anti-IL-2R, CS, MMF, Csa	1	0	Chronic rejection	214	C3
DTR20	81/M	+	71/F/White	Unknown	366	-	1	Anti-IL-2R, CS, MMF, Csa	0	0	Venous thrombosis	1	C1
DTR21	52/M	+	27/M/White	Cort Nec	1342	+	2	Anti-IL-2R, CS, MMF, FK506	6	0	Chronic rejection	1586	C3
DTR22	59/F	+	55/M/White	NAS	244	+	1	CS, Evero, Csa	1	0	Chronic rejection	519	C3
DTR23	57/F	+	25/F/White	Uropathy	765	+	1	Anti-IL-2R, CS, MMF, FK506	1	0	Chronic rejection	2372	C4
DTR24	49/M	+	18/M/Arab	Uropathy	1065	+	2	CS, Aza, Csa	2	0	Chronic rejection	3225	C4
DTR25	54/F	+	27/M/Arab	HUS	1467	-	2	ATG, CS, MMF, FK506	0	1	Chronic rejection	2732	C3
DTR26	61/M	-	35/M/White	ADPKD	743	-	1	Anti-IL-2R, CS, MMF, FK506	1	0	Chronic rejection	182	C3

A statistical analysis was performed to seek difference between the four clusters regarding the clinical characteristics of patients. No difference was found except for the number of acute cellular rejection (C1 = 0 versus C2 = 1.5 versus C3 = 1.2 versus C4 = 1; $\chi^2 = 8.548$; $p = 0.0359$).

^aThe CMV QRT-PCR performed on the cDNA of the 26 renal grafts were all negative, except for DTR12 (34,000 copies).

ADPKD, autosomal dominant polycystic kidney disease; Afr, African; Alport Sd, Alport syndrome; ATG, antithymocyte globulin; Aza, azathioprine; C, cadaveric; Cort Nec, cortical necrosis; CS, corticosteroid; Csa, cyclosporine A; ECGN, extracapillary glomerulonephritis; ESRF, end-stage renal failure; Evero, everolimus; FK506, tacrolimus; FSGS, focal segmental glomerulosclerosis; HSP, Henoch Schonlein purpura; HUS, hemolytic and uremic syndrome; IS regimen, immunosuppressive treatment; L, living; MGN, membranous glomerulopathy; MMF, mycophenolate mofetil; NAS, nephroangiosclerosis; No. AR, number of biopsy-proven episodes of acute rejection; No. CMV Dis, number of symptomatic CMV disease episodes; OKT3, anti-gCD3 Abs; Rank of Tr, rank of transplantation; Rec, recurrence; Siro, sirolimus; TMA, thrombotic microangiopathy.

Table II. List of primers

Gene	Sequences	Amplicon Length (bp)
<i>AID</i>	5'-CGTAGTGAAGAGGCGTGACA-3' 5'-TCAGACTGAGGTGGGGTTC-3'	227
<i>LTα</i>	5'-CACCGGAGCTTTCAAAGAAG-3' 5'-TGCTCTTCTCTGTGTGG-3'	175
<i>LTβ</i>	5'-TACGGGCTCTCTGGTACAC-3' 5'-ATATTCCCTCACCCACCAT-3'	155
<i>LTβR</i>	5'-ACCAGGTGTGAGAACCAGG-3' 5'-GAGCAGAAAGAAGGCCAGTG-3'	153
<i>CXCL12</i>	5'-TCAGCCTGAGCTACAGATGC-3' 5'-CTTTAGCTTCGGGTCAATGC-3'	161
<i>CXCR4</i>	5'-GGTGGTCTATGTTGGCGTCT-3' 5'-TGGAGTGTGACAGCTTGGAG-3'	227
<i>CXCL13</i>	5'-CTCTGCTTCTCATGCTGCTG-3' 5'-TGAGGGTCCACACACAAT-3'	220
<i>CXCR5</i>	5'-CCTCCCAGAACAACACTCCAT-3' 5'-TGCTTGGTCAAGATGACTGC-3'	229
<i>CCL21</i>	5'-GCCTTGCCACACTCTTTCTC-3' 5'-CAAGGAAGAGGTGGGGTGTGTA-3'	218
<i>CCL19</i>	5'-GGTGCCTGCTGTAGTGTCA-3' 5'-GGTCCTTCCTTCTGGTCTC-3'	220
<i>CCR7</i>	5'-GATGCGATGCTCTCTCATCA-3' 5'-TGTAGGGCAGCTGGAAGACT-3'	218
<i>GAPDH</i>	5'-GTGAAGGTCCGAGTCAAC-3' 5'-GGTGAAGACGCCAGTGGACTC-3'	294

marker (25) therefore indicating that the CD19^{pos}IgD^{pos}CD38^{neg} population includes both naive Bm1 cells (CD27^{neg}) and IgD^{pos} memory B cells (CD27^{pos}) (26). To exclude the possibility that memory B cells were underestimated when identified by their IgD/CD38 expression, we compared the proportion of CD19^{pos}

CD27^{pos} cells. We found a gradual increase in CD27^{pos} B cells, from C2 to C4, further validating the results obtained with the Bm1–Bm5 classification (Fig. 3C).

Finally, kidneys from the C2 cluster can be regarded as inflamed tissues in which the maturation of naive B cells is the less efficient; whereas, the C4 cluster gathers samples in which naive B cells are the most efficiently converted into memory B cells (Student *t* test = 3.23; *p* = 0.001). We therefore conclude that the progression of B cells through the successive maturation stages correlates with the gene expression profile of the inflamed tissue.

Clusters correlate with the intensity of the local immune responses

During germinal center reaction, high-affinity B cells are converted into plasmacells, which secrete large amounts of Abs. Plasmacells, easily identifiable by the expression of Syndecan-1 (CD138) and the presence in their cytoplasm of large, eosinophilic, homogenous inclusions, known as Russell bodies, were evidenced in the periphery of eGC (Fig. 4A). In accordance, plasmacells, defined as CD38^{ultrabright}CD138^{pos}, were also detected in the samples from the C3 and C4 clusters (Fig. 4B), namely, the two clusters comprising the samples in which 1) lymphoid organogenesis genes were highly expressed (Fig. 2A), 2) eGCs were detected histologically (Fig. 2C), and 3) the local maturation of B cells was the most efficient (Fig. 3B). This strongly suggests that the gene expression profile of the inflamed tissue determines the progression of B cells through the successive maturation stages. To test this hypothesis, the production of Ig was quantified in tissue-culture conditioned media. Quantification of the various classes and subclasses of Ig produced locally was performed by ELISA in the supernatants after 5 d of tissue culture. IgA and IgM were not detected (data not shown). In contrast, a local production of IgG (Fig. 4C), which increased gradually from the C1 to the C4 samples, was found (Student *t* test = 2.26; *p* = 0.024). There was no difference regarding IgG subclass distribution in the samples from the various clusters (Fig. 4D). One limitation of using ELISA to detect IgG on tissue-culture supernatants is the impossibility of discriminating between IgG, which might be trapped within the tissue and subsequently released, from IgG produced by infiltrated plasmacells. Indeed,

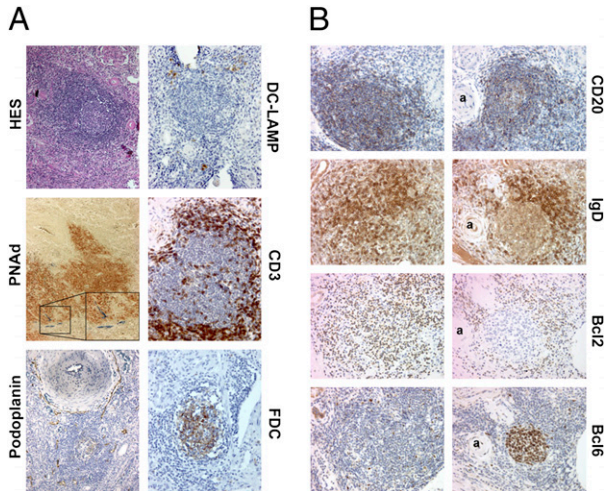


FIGURE 1. Persistent immune activation triggers the development of heterogeneous nodular B cell structures in inflamed tissues. *A*, Systematic histological analysis was carried out on sections of kidney grafts explanted because of terminal failure. Representative findings characterizing chronically rejected grafts are shown. H&E staining showed the nodular organization of the inflammatory infiltrate. PNA and podoplanin immunostaining revealed the high endothelial venule and lymphatic networks, respectively, surrounding the nodules. The spatial organization of cell populations was analyzed by immunohistochemistry with Abs directed to FDC, CD3 (T cells), and DC-LAMP (mature dendritic cells) (original magnification $\times 200$). *B*, Nodules were composed of a core of CD20^{pos} cells. Most of the nodules were composed of a homogenous B cell population expressing IgD and Bcl-2 but no Bcl-6 (left column, hereafter referred to as primary follicle-like nodules). In certain nodules (right column, hereafter referred to as eGCs), this B cell population was driven toward the periphery by CD20^{pos} IgD^{neg} Bcl-2^{neg} cells expressing Bcl-6 now occupying the center of the nodule (original magnification $\times 400$). a, the same arteriole on the successive serial sections; FDC, follicular dendritic cells.

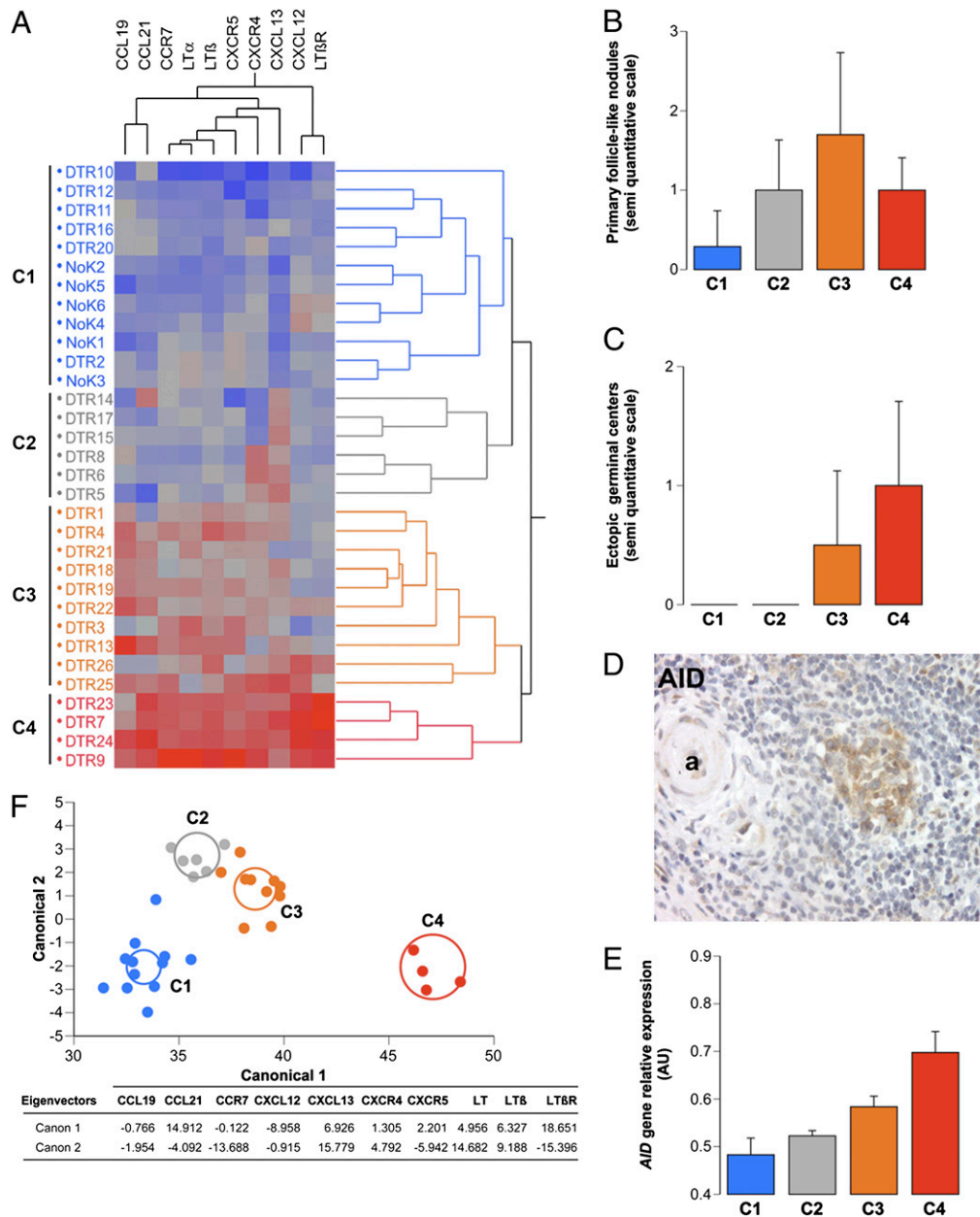


FIGURE 2. Lymphoid neogenesis is a recapitulation of the embryonic lymphoid organogenesis program. **A**, For each kidney, mRNA was extracted from two distinct tissue fragments and reverse transcribed. For each gene involved in lymphoid organogenesis, real-time QRT-PCR was run five times on each cDNA preparation. Expression levels of these genes were normalized to that of the GAPDH housekeeping gene. For each gene, the 10 values obtained for a single kidney were averaged and the data set was computed to clusterize tissues according to their expression pattern (Ward hierarchical clustering). Individual samples are listed in rows, the genes in columns, and increasing expression levels are encoded from dark blue to bright red. On the top and on the right of the color map, dendrograms list each observation, and indicate the cluster it is in and when it entered its cluster. Four clusters C1–C4 were identified. **B** and **C**, The number of primary follicle-like nodules (**B**) and eGCs (**C**) was evaluated blindly by a pathologist (N.P.) using a semiquantitative scale ranging from 0 (samples without follicle/eGC) to 3 (samples with >5 follicles/eGCs per field) (original magnification $\times 50$). For each sample, 10 sections from four distinct paraffin-embedded blocks were analyzed. For the analysis, histological quantifications were grouped according to the gene expression-defined clusters (mean \pm SD). **D**, AID protein expression analysis was performed by immunohistochemistry. This staining, performed on the successive serial sections used for the immunohistological study presented in Fig. 1B (a, the same arteriole as in the sections of Fig. 1B), shows that AICD expression is restricted to the germinal center B cell population (CD20^{pos}IgD^{neg}Bcl2^{neg}Bcl6^{pos}) (original magnification $\times 400$). AID was not expressed by the CD20^{pos}IgD^{pos}Bcl2^{pos}Bcl6^{neg} B cells, either in the periphery of eGCs or in primary follicle-like nodules. **E**, The expression level of *AID* was analyzed by real-time QRT-PCR with the same methods described in the Fig. 2A legend (mean \pm SD). **F**, The principal component analysis was used to reduce the multidimensional gene expression data set to lower dimensions for analysis, by retaining those characteristics of the data set that contributed most to its variance. The projection of the data on the first and second principal components (canonical 1 and 2) efficiently discriminated the four clusters when individual samples were projected orthogonally. Each circle represents the multivariate mean for each cluster and the size of the circle corresponds to a 95% confidence limit. Nonintersecting circles indicate that clusters are significantly different; however, the difficulty to discriminate between the C2 and C3 clusters suggests that these two clusters are closely related. The composition of the eigenvectors, indicated in the Table below the graph, revealed that the chemokines CCL21 and CXCL13, and the *LTβR*, were the genes with the largest eigenvalues, namely, the genes that contributed most to dividing the samples into the four clusters. LT, lymphotoxin; NoK, normal kidney.

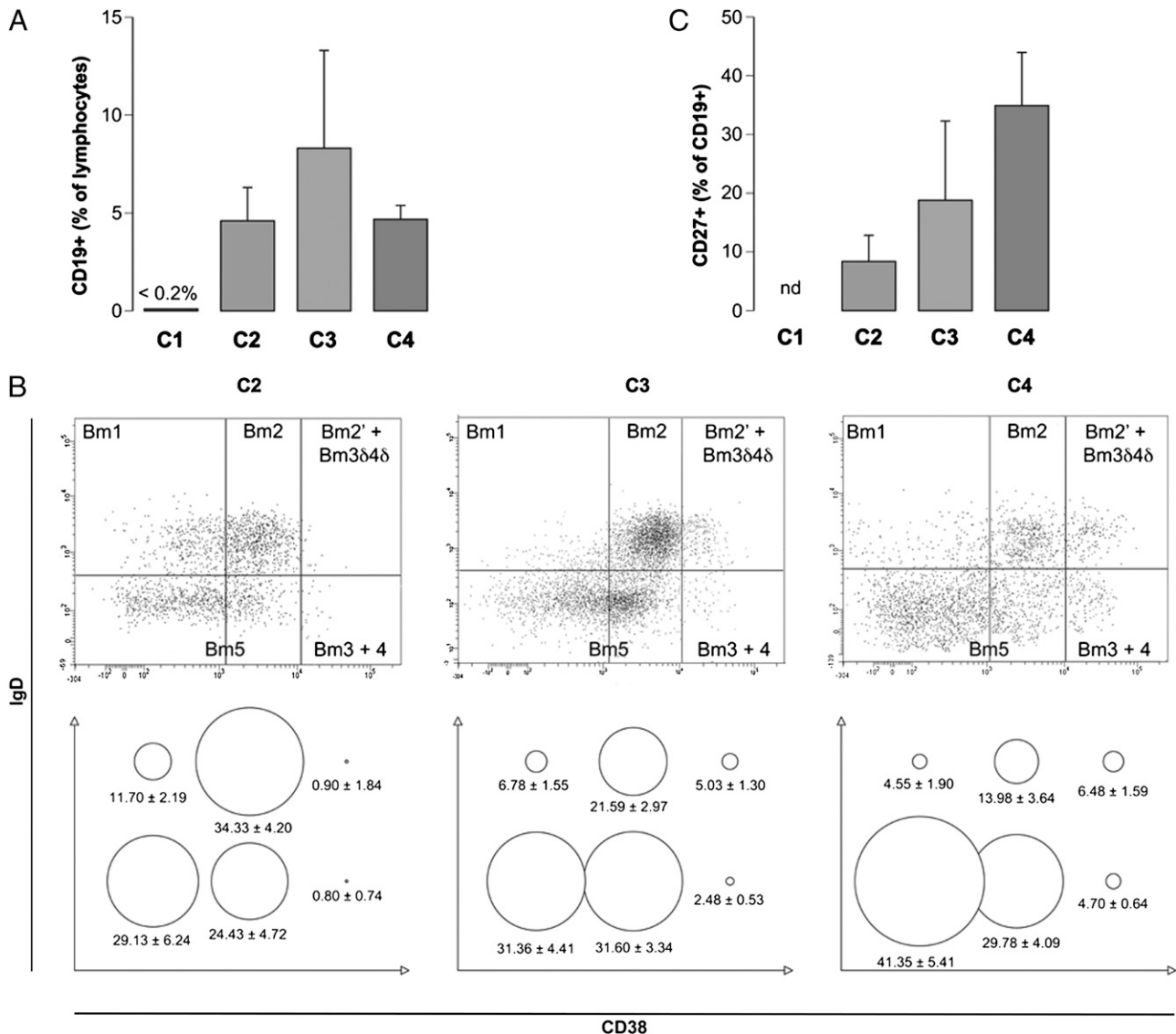


FIGURE 3. Incomplete recapitulation of the program impedes local B cell maturation. Tissue samples were processed to isolate the inflammatory infiltrate which was then analyzed by polychromatic flow cytometry. *A*, The percentage of CD19^{pos} B cells among lymphocytes (identified on the FSC/SSC morphology gating) is provided for each cluster. Note that the inflammatory infiltrate in the samples from the C1 cluster was minimal and B cells were barely detectable (mean \pm SD). *B*, B cell maturation stages were identified on the basis of the IgD/CD38 staining of CD19^{pos} cells in the C2 (*left*), C3 (*middle*), and C4 (*right*) clusters (dot plots from three representative samples). The Bm1 and Bm2 naive cells are IgD^{pos}CD38^{neg} and IgD^{pos}CD38^{dim}, respectively. The Bm2' and Bm3 δ 4 δ pregerminal center B cells are IgD^{pos}CD38^{bright}; the Bm3 and Bm4 germinal center B cells are IgD^{neg}CD38^{bright}. The early and late Bm5 are, respectively, IgD^{neg}CD38^{dim} and IgD^{neg}CD38^{neg}. The gating that was used excluded the CD38^{ultrabright} from the present analysis. The bubble graphs below the dot plots represents the average percentage of each type of B cell (mean \pm SD). *C*, The percentage of CD27^{pos} cells among CD19^{pos} cells was used to quantify memory B cells. In the samples from the C1 cluster, the paucity of the infiltrate made the assessment of memory B cells unreliable. nd, not determined.

a small amount of IgG was detected in the C1 cluster samples (Fig. 4C), in which plasmacells were absent (Fig. 4B). We therefore performed an ELISPOT assay on representative samples from the C3 and C4 clusters that demonstrated the presence of IgG-producing cells among the inflammatory infiltrate (Fig. 4E). The increased number of spots observed on mitogen stimulation in the C4, as compared with the C3 cluster (Fig. 4E), indicated that the number of memory B cells was higher in the C4 samples, in accordance with the results of flow cytometric analysis (Fig. 3B, 3C).

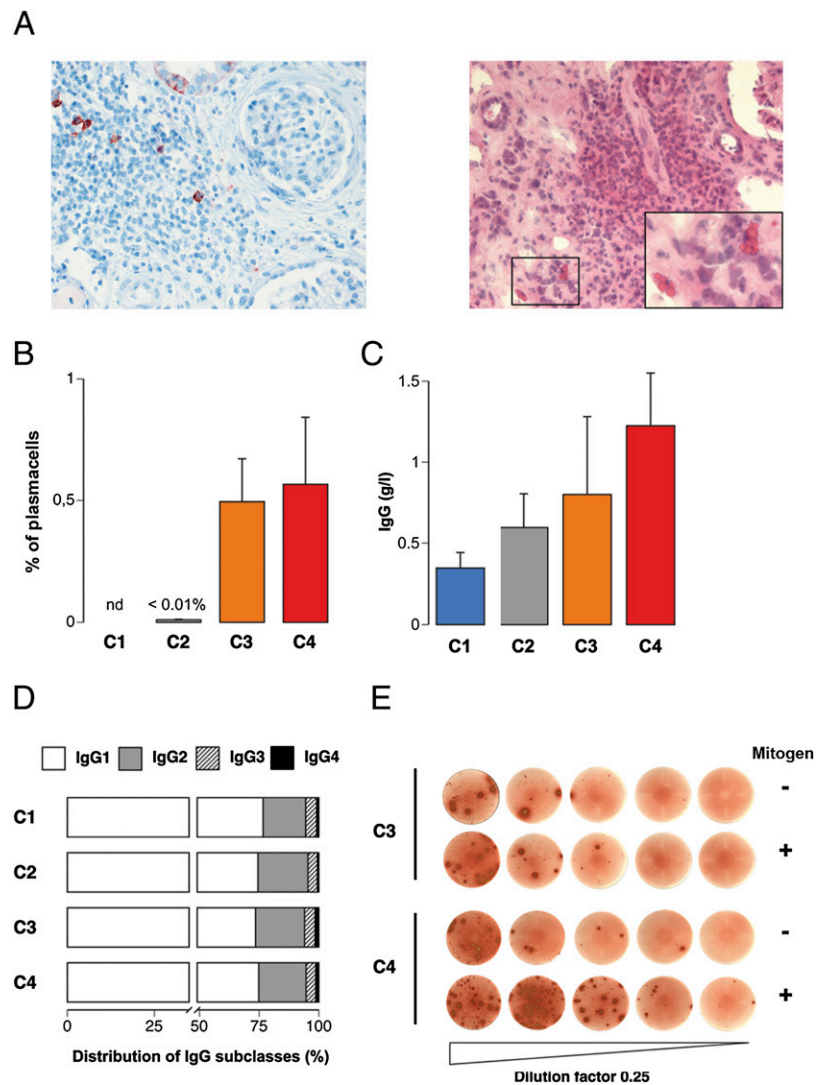
Clusters correlate with the aggressiveness of the local alloimmune response

For 18 of 26 of the explanted kidneys, 24 randomly selected cortical fragments per kidney were tissue cultured and the supernatants

were collected after 5 d. The quantification of anti-HLA Abs in these supernatants by luminex assays allowed us to characterize the local alloimmune response as follows: 1) the density of the response was defined as the percentage of wells that were positive for either HLA I or HLA II; 2) the diversity was the ratio of the number of specificities over the number of HLA mismatches for each donor/recipient couple; and 3) the intensity was the highest mean fluorescence intensity (MFI).

As expected, there were no alloantibodies in the tissue supernatants from the C1 cluster. In contrast, a local production of antidonor Abs was detected in the tissues of the three remaining clusters. The density, diversity, and intensity of the local humoral response against the target Ags (Table III) were maximal in the C4 cluster and minimal in the C2 cluster (Student *t* test = 4.62;

FIGURE 4. Complete recapitulation of the program leads to development of fully functional eGCs. *A*, Plasmacells were evidenced in the periphery of eGC by the expression of CD138 (*left panel*) and the presence in their cytoplasm of large pathognomonic, eosinophilic, homogenous inclusions, known as Russell bodies, on H&E staining (*right panel*) (original magnification $\times 200$). *B*, The percentage of CD38^{ultrabright} CD138^{pos} plasmacells infiltrating the graft analyzed by flow cytometry is represented. *C* and *D*, For each explanted kidney, tissue cultures of 24 cortical fragments were performed in 24-well plates in 1 ml serum-free RPMI 1640. Supernatants were collected after 5 d. The content of total IgG was measured in duplicate in two randomly selected supernatants by ELISA (*C*) (mean \pm SD). The subclasses of IgG were quantified in duplicate in the same supernatants by ELISA (*D*). The values are expressed as the percentage of the total amount of IgG. *E*, Quantification of IgG-producing cells (plasmacells and stimulated memory B cells) was carried out by an ELISPOT assay on two randomly selected samples from the C3 and C4 clusters. Given that CD38^{ultrabright}CD138^{pos} cells were not detected by flow cytometry in the samples from the C1 and C2 clusters, ELISPOT assays were not run on cells from these samples. Representative findings are shown. Cells extracted from explanted kidneys were cultured for 6 d in complete medium with or without a B cell mitogen mix (PWM, SAC, CpG). Cells were plated 6 h in cascade 1/4 dilutions in multiscreen 96-well filter plates coated with anti-human IgG Abs. Spots were revealed with biotinylated goat anti-human IgG Fc, HRP-conjugated Avidin D, and 3-amino-9-ethyl-carbazole. Unstimulated wells allow for evaluation of plasmacells; mitogen-treated wells allow for that of memory B cells.



$p < 0.001$). The diversity and intensity of the local alloimmune response in the C2 and C3 clusters were similar. This is consistent with the close relation between of these two clusters, as demonstrated by the principal component analysis (Fig. 2F). These two clusters only differed in density.

Local humoral response is uncoupled from the systemic response

Alloantibodies produced in “canonical” secondary lymphoid organs (i.e., the spleen and the lymph nodes) reach the graft through the circulation. Analysis of the serum therefore offers a unique opportunity to compare the local (i.e., intra-graft) and the systemic (i.e., elicited in the secondary lymphoid organs) humoral alloimmune responses. The luminex assays performed on the sera collected at the time of the explantation demonstrated a disconnection between systemic and local humoral responses. Indeed, Ab specificities found in tissue-culture supernatants were almost systematically distinct from those detected in the sera (Fig. 5A, Table III). Also, the local response appeared more diverse, especially in the C4 samples (Fig. 5A, Table III).

Functionality of intra-graft lymphoid tissue and graft survival

Because we observed that grafts of the C2 cluster had functioned 7.8 y on average and those of the C4 cluster had lasted only half that time (3.5 y; Fig. 5B); whereas we found no statistically significant difference between the clusters for the clinical characteristics that

could explain this difference (Table I), we put forward the hypothesis that the functionality of intra-graft lymphoid tissue could negatively impact graft survival. A first analysis documented a statistical difference in graft survival between the four clusters ($\chi^2 = 30.08$; $p < 0.0001$). However, this difference was likely related to the very short survival of samples from the C1 cluster (three samples of this group were explanted for primary surgical failure). Therefore, in an attempt to more specifically explore the influence of gene expression-based clusterization on chronic rejection kinetic, we performed a subgroup analysis on chronically rejected grafts only (samples from C1 cluster were excluded). Interestingly, this subgroup analysis ($\chi^2 = 5.96$; $p = 0.0507$) almost reached the statistical significance despite the very low number of patients of the study.

Discussion

In the current study, we have performed a comprehensive analysis of the molecular and cellular events that take place in human chronically rejected grafts in which lymphoid neogenesis is invariably observed (11, 12).

We observed that the expression of lymphoid organogenesis genes was heterogeneous in chronically rejected allografts. Hierarchical clusterization of the QRT-PCR dataset was used to sort the samples into four clusters according to their pattern of expression for lymphoid organogenesis genes. The C1 cluster contained all the control

Table III. Density, diversity, and intensity of the local humoral alloimmune response

	A/B/DR Mismatches	Density of the Local Immune Response		Diversity of the Immune Response		Intensity of the Local Immune Response MFI Max/MFI Control
		Anti-HLA I	Anti-HLA II	Total (%)	Local (Nb Specificities/Nb Mismatches)	
DTR10	A29 B13 B72 DR13 DR16	0/23	0/23	0	0	0
DTR11	No mismatch	0/24	0/24	0	0	0
DTR12	DR8 DR13	0/23	0/23	0	0	1 (DR11 DQ2)
DTR16	A25 B65 DR1	0/23	0/23	0	0	0.3 (A25)
DTR20	A31 B7 B37 DR11	0/24	0/24	0	0	0
C1				0 ± 0	0	0.3 ± 0.4
DTR14	A26 B7 B53 DR1 DR10	7/22	0/22	31.8	1 (A26 A3 A11 B59 B67)	0.4 (B53 DR103)
DTR15	A2 DR6 DR7	8/23	10/23	43.5	1 (A2 DR7 A68)	0.3 (A2)
DTR17	B27 DR8 DR14	0/23	8/23	37.8	1.3 (DR8 DQ2 DQ3 DQ4)	0
C2				37.7 ± 5.9	1.1 ± 0.2	0.2 ± 0.2
DTR13	A1 A33 B51 B35 DR13	0/11	0/11	0	0	0
DTR18	B7 B37	0/23	23/23	100	1 (DR3 DR7)	2 (DR3 DR5 DR6 DR8)
DTR19	A2 B51 B62 DR3 DR4	0/23	0/23	0	0	0
DTR21	A31 B51	20/23	15/23	87	2.5 (A25, 26, 34, 66 DR13)	1 (DR8 DR103)
DTR22	A3 A26 B52 DR15	0/22	0/22	0	0	0
DTR25	A26 B35 B38 DR1	12/12	0/12	100	0.5 (B35 DR1)	0
DTR26	B51	12/12	0/12	100	1 (B51)	0
C3				55.3 ± 51.9	0.7 ± 0.9	0.4 ± 0.8
DTR9	A2 DR7	29/32	0/32	90.6	3 (A2 A26 A29 A32 A68 A69)	3 (A2 A29 A32 A33 A68 A69)
DTR23	A3 A26 B51 DR13 DR4	23/23	23/23	100	6.4 (32 specificities)	3 (15 specificities)
DTR24	B17 B44 DR4	23/23	23/23	100	19.3 (58 specificities)	0.3 (A25)
C4				96.9 ± 5.4	9.6 ± 8.6	2.1 ± 1.5

Twenty four fragments of randomly sampled renal cortex were tissue cultured. Because this part of the study was initiated after DTR8, data concerning DTR1-DTR8 are lacking. Anticlass II HLA Abs were sought for in the supernatants of tissue cultures and in the sera obtained immediately before de transplantation by the luminex detection kit. We defined the density of the local humoral alloimmune response as the percentage of wells positive for either HLA I or HLA II. We subsequently measured the diversity and the intensity of the local humoral immune response using the luminex single Ag kit on the supernatant from the well displaying the highest MFI in the luminex detection kit. The diversity of the peripheral humoral response was measured on the sera obtained immediately before de transplantation. The diversity of the immune response was calculated as the number of detected specificities normalized by the number of HLA mismatches for the donor/recipient pair. The intensity of the local humoral immune response was defined as the maximal MFI observed, normalized by the MFI of the positive control. Direct comparison of the density and the intensity of the local and peripheral humoral responses is not possible. Bold text corresponds to the mean of each cluster (C1, C2, C3, and C4).

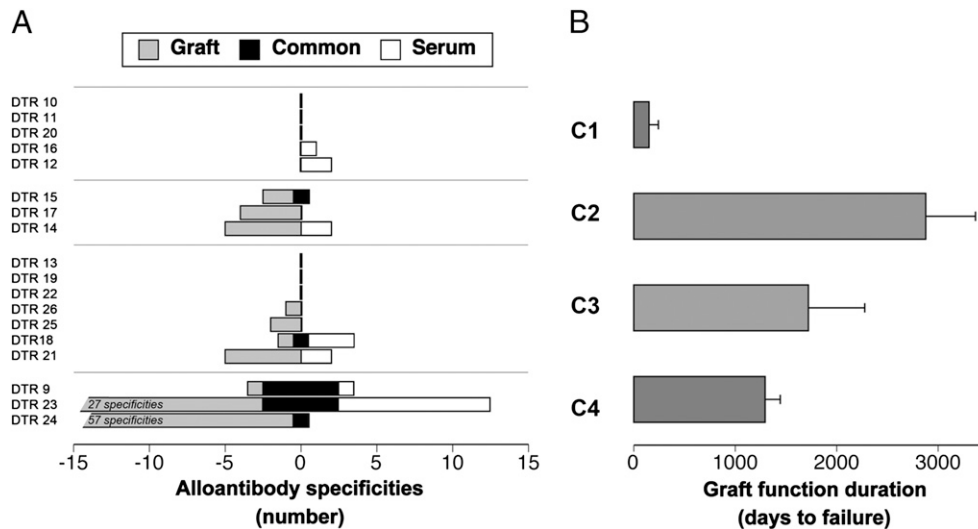


FIGURE 5. Local and systemic humoral alloimmune responses are uncoupled. *A*, Anticlass I and anticlass II HLA Abs were identified by the luminex single Ag kit (see Table III legend) in the supernatants of tissue cultures (grey bars) and in the sera obtained immediately before detransplantation (white bars). The black bars represents the specificities detected simultaneously in the serum and the supernatants of tissue cultures. Because this part of the study was initiated after DTR8, data concerning DTR1 to DTR8 are lacking. *B*, The duration of graft function, set as the number of days between transplantation and the return to dialysis, was plotted for the four clusters of DTRs (mean \pm SD).

tissues (six normal kidneys, three grafts explanted due to primary surgical failure, and three grafts explanted due to nonimmune mediated failure). Rejected grafts were distributed among three additional clusters of expression patterns (C2–C4). These three different clusters could either reflect distinct biological programs or, alternatively, they might identify different stages of the same program. Although the design of the current study does not allow us to draw a definitive conclusion regarding these two hypotheses, several findings point toward the latter possibility. Indeed, gene expression is not randomly distributed: C2 differs from C1 by switching on a limited number of genes, C3 is characterized by the expression of additional genes compared with C2, and finally C4 contains the samples that express all the genes involved in lymphoid organogenesis. This suggests that the development of a functional ectopic tertiary lymphoid tissue during chronic inflammation has to go through three checkpoints. The C1–C2 checkpoint involves the expression of *CXCL13* and *CXCR4*. The progression from C2 to C3 requires the additional expression of *CCL19*, *CCL21*, *CCR7*, *LT α* , *LT β* , and *CXCR5*. Complete recapitulation of the lymphoid organogenesis program is finally achieved with the supplementary expression of *CXCL12* and *LT β* R, which characterizes the transition from C3 to C4. The complete recapitulation of this program results in the generation of fully functional eGCs, which allows for the efficient maturation of B cells up to memory B cells and plasmacells. In contrast, when this recapitulation was incomplete, local B cell maturation was impeded. Statistical analysis on this small cohort found no influence of immunosuppressive treatments on lymphoid neogenesis. Indeed, neither the administration of an induction therapy, nor the nature of the immunosuppressive regimen (anticalcineurin-based versus mammalian target of rapamycin-inhibitor based) showed any influence on the distribution of the patients across the four clusters.

Interestingly, we observed a trend ($p = 0.0507$) for a shorter survival for the grafts of the C4 cluster, which lasted 3.5 y in average as compared with 7.8 y for the C2 cluster. These preliminary results, in line with previous experimental studies (27), suggest a detrimental role of lymphoid neogenesis that could hasten chronic destruction of the graft. However, given the small number of grafts analyzed and the limitations inherent to statis-

tical subgroup analysis, additional work is required to definitively validate this hypothesis.

We found that the specificities of circulating Abs were different from those of locally produced Abs. This implies that there are two compartmentalized immune responses that each target distinct Ags. The higher diversity of the local response points to a laxer selection process of B cell clones in eGCs. These observations provide interesting clues regarding the reasons why evolution have kept in mammals the ancestral capacity to mount a local immune response in the presence of secondary lymphoid organs, the canonic place for the elicitation of adaptive immune responses. Because lymphoid neogenesis generates effectors close to their targets and displaying original specificities, it may provide selective advantage to prevent dissemination of pathogens resistant to “classical” responses. In contrast, the higher aggressiveness of the local response implies that it may be more difficult to control by standard therapeutic strategies. In line with this hypothesis, we (28) and others (29) have recently shown that tertiary lymphoid tissues B cells could survive anti-CD20 Ab (rituximab) therapy when circulating B cells were efficiently depleted. The current study paves the way for innovative therapeutic strategies aimed at blocking the maturation of local adaptive immune response. Indeed, among the molecular checkpoints, critical for the completion of the lymphoid neogenesis program, that we have identified, *LT β* R represents an attractive therapeutic target. *LT β* R signaling primes the expression of homeostatic chemokines in stromal cells (30), and therefore plays a critical role in the recruitment and subsequent organization of inflammatory effectors within the diseased tissue (6, 31–35). Our findings, which demonstrate that *LT β* R expression is characteristic of samples from the C4 cluster, indicate that its role is not restricted to the early stages of the ontogeny of lymphoid organs; it also extends to the maintenance of lymphoid-tissue architecture as proposed by Browning et al. (36). In addition, *LT β* R has been shown to orchestrate lymphangiogenesis (37) that could fuel lymphoid neogenesis by carrying the antigenic information to the neoformed eGCs (38).

The current study was performed on explanted organs, namely, on grafts that had failed. This choice constitutes a limitation of the current study that precluded a kinetic analysis of the process. In contrast, the large amount of tissue allowed simultaneous analyzes

at both the molecular and cellular levels that provided valuable and novel information about maturation stages of the intragraft immune response. Further, our results obtained on grafts with terminal failure indicate a detrimental role of lymphoid neogenesis during chronic inflammation, a conclusion not reached by biopsy-based studies (39–41). Two explanations can be proposed to reconcile these apparently conflicting results. First, not only are the data provided by the biopsies limited to a small area of tissue, but this small amount of tissue does not allow for functional analysis of the ectopic lymphoid organs. In our experience, histological analysis (even on a large area) was of limited value for discriminating samples of the C4 cluster from those of the C2 cluster. For example, despite the fact that histological analysis was performed on 10 fields from four different blocks, it failed to document lymphoid nodules in the interstitium of DTR17. It is, however, likely that a low number of functional eGCs were present in this chronically rejected graft because: 1) CD19⁺ B cells were detected by flow cytometry, 2) QRT-PCR demonstrated a low but significant AICD expression, and 3) tissue-culture experiments evidenced a local production of Abs in 38% of the tissue-culture supernatants for this sample. Therefore, although irreplaceable to obtain topological information regarding ectopic lymphoid nodules, histology is not accurate to quantify lymphoid neogenesis.

An alternative, though not entirely exclusive, hypothesis is that in some situations, lymphoid neogenesis could generate a regulatory and protective immune response. This theory, which arose from the clinical observations of lymphoid aggregates in allografts devoid of rejection lesion (42), has been further substantiated by recent experimental findings. Indeed, Katakai et al. (43) have shown that the development of tertiary lymphoid tissue correlated with a marked limitation of tissue damage in a murine model of autoimmune gastritis. Finally, a number of recent publications point to the immune regulatory role of certain B cell subsets (44, 45). If such a protective response is able to prevent terminal failure of grafts, then such samples with “tolerogenic” lymphoid neogenesis would be absent from our study. Developing future therapeutic strategies targeting lymphoid neogenesis to prevent chronic inflammation will therefore require prior determination of whether it is desirable to block or to deviate the local immune response.

Acknowledgments

This work is dedicated to the memory of Sophie Lechaton. We thank the urologists, pathologists, and nephrologists from the Foch, Henri Mondor, Necker, and Pasteur Hospitals for assistance in the collection of the samples. We thank Anne Durandy for anti-AID Abs.

Disclosures

The authors have no financial conflicts of interest.

References

- Rosenberg, H. F., and J. I. Gallin. 2003. Inflammation. In *Fundamental Immunology*, 5th Ed., W. E. Paul, ed. Lippincott Williams & Wilkins, Philadelphia.
- Prineas, J. W. 1979. Multiple sclerosis: presence of lymphatic capillaries and lymphoid tissue in the brain and spinal cord. *Science* 203: 1123–1125.
- Kratz, A., A. Campos-Neto, M. S. Hanson, and N. H. Ruddle. 1996. Chronic inflammation caused by lymphotoxin is lymphoid neogenesis. *J. Exp. Med.* 183: 1461–1472.
- Drayton, D. L., S. Liao, R. H. Mounzer, and N. H. Ruddle. 2006. Lymphoid organ development: from ontogeny to neogenesis. *Nat. Immunol.* 7: 344–353.
- Gause, A., K. Gundlach, M. Zdechavsky, G. Jacobs, B. Koch, T. Hopf, and M. Pfreundschuh. 1995. The B lymphocyte in rheumatoid arthritis: analysis of rearranged V kappa genes from B cells infiltrating the synovial membrane. *Eur. J. Immunol.* 25: 2775–2782.
- Hjelmström, P., J. Fjell, T. Nakagawa, R. Sacca, C. A. Cuff, and N. H. Ruddle. 2000. Lymphoid tissue homing chemokines are expressed in chronic inflammation. *Am. J. Pathol.* 156: 1133–1138.
- Schröder, A. E., A. Greiner, C. Seyfert, and C. Berek. 1996. Differentiation of B cells in the nonlymphoid tissue of the synovial membrane of patients with rheumatoid arthritis. *Proc. Natl. Acad. Sci. USA* 93: 221–225.
- Aloisi, F., and R. Pujol-Borrell. 2006. Lymphoid neogenesis in chronic inflammatory diseases. *Nat. Rev. Immunol.* 6: 205–217.
- Kerjaschki, D., H. M. Regele, I. Moosberger, K. Nagy-Bojarski, B. Watschinger, A. Soleiman, P. Birner, S. Krieger, A. Hovorka, G. Silberhumer, et al. 2004. Lymphatic neovascularization in human kidney transplants is associated with immunologically active lymphocytic infiltrates. *J. Am. Soc. Nephrol.* 15: 603–612.
- Baddoura, F. K., I. W. Nasr, B. Wrobel, Q. Li, N. H. Ruddle, and F. G. Lakkis. 2005. Lymphoid neogenesis in murine cardiac allografts undergoing chronic rejection. *Am. J. Transplant.* 5: 510–516.
- Thaunat, O., A. C. Field, J. Dai, L. Louedec, N. Patey, M. F. Bloch, C. Mandet, M. F. Belair, P. Pruneval, O. Meilhac, et al. 2005. Lymphoid neogenesis in chronic rejection: evidence for a local humoral alloimmune response. *Proc. Natl. Acad. Sci. USA* 102: 14723–14728.
- Thaunat, O., N. Patey, E. Morelon, J. B. Michel, and A. Nicoletti. 2006. Lymphoid neogenesis in chronic rejection: the murderer is in the house. *Curr. Opin. Immunol.* 18: 576–579.
- Crotty, S., R. D. Aubert, J. Glidewell, and R. Ahmed. 2004. Tracking human antigen-specific memory B cells: a sensitive and generalized ELISPOT system. *J. Immunol. Methods* 286: 111–122.
- Mamani-Matsuda, M., A. Cosma, S. Weller, A. Faili, C. Staib, L. Garçon, O. Hermine, O. Beyne-Rauzy, C. Fieschi, J. O. Pers, et al. 2008. The human spleen is a major reservoir for long-lived vaccinia virus-specific memory B cells. *Blood* 111: 4653–4659.
- Wagner, U. G., P. J. Kurtin, A. Wahner, M. Brackertz, D. J. Berry, J. J. Goronzy, and C. M. Weyand. 1998. The role of CD8+ CD40L+ T cells in the formation of germinal centers in rheumatoid synovitis. *J. Immunol.* 161: 6390–6397.
- Ansel, K. M., V. N. Ngo, P. L. Hyman, S. A. Luther, R. Förster, J. D. Sedgwick, J. L. Browning, M. Lipp, and J. G. Cyster. 2000. A chemokine-driven positive feedback loop organizes lymphoid follicles. *Nature* 406: 309–314.
- Cyster, J. G. 2003. Lymphoid organ development and cell migration. *Immunol. Rev.* 195: 5–14.
- Fütterer, A., K. Mink, A. Luz, M. H. Kosco-Vilbois, and K. Pfeffer. 1998. The lymphotoxin beta receptor controls organogenesis and affinity maturation in peripheral lymphoid tissues. *Immunity* 9: 59–70.
- Mebius, R. E. 2003. Organogenesis of lymphoid tissues. *Nat. Rev. Immunol.* 3: 292–303.
- Rennert, P. D., J. L. Browning, R. Mebius, F. Mackay, and P. S. Hochman. 1996. Surface lymphotoxin alpha/beta complex is required for the development of peripheral lymphoid organs. *J. Exp. Med.* 184: 1999–2006.
- Rennert, P. D., D. James, F. Mackay, J. L. Browning, and P. S. Hochman. 1998. Lymph node genesis is induced by signaling through the lymphotoxin beta receptor. *Immunity* 9: 71–79.
- De Togni, P., J. Goellner, N. H. Ruddle, P. R. Streeter, A. Fick, S. Mariathan, S. C. Smith, R. Carlson, L. P. Shornick, J. Strauss-Schoenberger, et al. 1994. Abnormal development of peripheral lymphoid organs in mice deficient in lymphotoxin. *Science* 264: 703–707.
- Humby, F., M. Bombardieri, A. Manzo, S. Kelly, M. C. Blades, B. Kirkham, J. Spencer, and C. Pitzalis. 2009. Ectopic lymphoid structures support ongoing production of class-switched autoantibodies in rheumatoid synovium. *PLoS Med.* 6: e1.
- Pascual, V., Y. J. Liu, A. Magalski, O. de Bouteiller, J. Banchereau, and J. D. Capra. 1994. Analysis of somatic mutation in five B cell subsets of human tonsil. *J. Exp. Med.* 180: 329–339.
- Agematsu, K., S. Hokibara, H. Nagumo, and A. Komiyama. 2000. CD27: a memory B-cell marker. *Immunol. Today* 21: 204–206.
- Bohnhorst, J. O., M. B. Björger, J. E. Thoen, J. B. Natvig, and K. M. Thompson. 2001. Bm1-Bm5 classification of peripheral blood B cells reveals circulating germinal center founder cells in healthy individuals and disturbance in the B cell subpopulations in patients with primary Sjögren's syndrome. *J. Immunol.* 167: 3610–3618.
- Columba-Cabezas, S., M. Griguoli, B. Rosicarelli, R. Magliozzi, F. Ria, B. Serafini, and F. Aloisi. 2006. Suppression of established experimental autoimmune encephalomyelitis and formation of meningeal lymphoid follicles by lymphotoxin beta receptor-Ig fusion protein. *J. Neuroimmunol.* 179: 76–86.
- Thaunat, O., N. Patey, C. Gautreau, S. Lechaton, V. Fremereaux-Bacchi, M. C. Dieunot-Neau, E. Cassuto-Viguier, C. Legendre, M. Delahousse, P. Lang, et al. 2008. B cell survival in intragraft tertiary lymphoid organs after rituximab therapy. *Transplantation* 85: 1648–1653.
- Kavanaugh, A., S. Rosengren, S. J. Lee, D. Hammaker, G. S. Firestein, K. Kalunian, N. Wei, and D. L. Boyle. 2008. Assessment of rituximab's immunomodulatory synovial effects (ARISE trial). I: clinical and synovial biomarker results. *Ann. Rheum. Dis.* 67: 402–408.
- Dejardin, E., N. M. Droin, M. Delhase, E. Haas, Y. Cao, C. Makris, Z. W. Li, M. Karin, C. F. Ware, and D. R. Green. 2002. The lymphotoxin-beta receptor induces different patterns of gene expression via two NF-kappaB pathways. *Immunity* 17: 525–535.
- Carlsen, H. S., E. S. Bækkevold, H. C. Morton, G. Haraldsen, and P. Brandtzaeg. 2004. Monocyte-like and mature macrophages produce CXCL13 (B cell-attracting chemokine 1) in inflammatory lesions with lymphoid neogenesis. *Blood* 104: 3021–3027.
- Corcione, A., S. Casazza, E. Ferretti, D. Giunti, E. Zappia, A. Pistorio, C. Gambini, G. L. Mancardi, A. Uccelli, and V. Pistoia. 2004. Recapitulation of

- B cell differentiation in the central nervous system of patients with multiple sclerosis. *Proc. Natl. Acad. Sci. USA* 101: 11064–11069.
33. Manzo, A., S. Paoletti, M. Carulli, M. C. Blades, F. Barone, G. Yanni, O. Fitzgerald, B. Bresnihan, R. Caporali, C. Montecucco, et al. 2005. Systematic microanatomical analysis of CXCL13 and CCL21 in situ production and progressive lymphoid organization in rheumatoid synovitis. *Eur. J. Immunol.* 35: 1347–1359.
 34. Salomonsson, S., P. Larsson, P. Tengnér, E. Mellquist, P. Hjelmström, and M. Wahren-Herlenius. 2002. Expression of the B cell-attracting chemokine CXCL13 in the target organ and autoantibody production in ectopic lymphoid tissue in the chronic inflammatory disease Sjögren's syndrome. *Scand. J. Immunol.* 55: 336–342.
 35. Takemura, S., A. Braun, C. Crowson, P. J. Kurtin, R. H. Cofield, W. M. O'Fallon, J. J. Goronzy, and C. M. Weyand. 2001. Lymphoid neogenesis in rheumatoid synovitis. *J. Immunol.* 167: 1072–1080.
 36. Browning, J. L., N. Allaire, A. Ngam-Ek, E. Notidis, J. Hunt, S. Perrin, and R. A. Fava. 2005. Lymphotoxin-beta receptor signaling is required for the homeostatic control of HEV differentiation and function. *Immunity* 23: 539–550.
 37. Furtado, G. C., T. Marinkovic, A. P. Martin, A. Garin, B. Hoch, W. Hubner, B. K. Chen, E. Genden, M. Skobe, and S. A. Lira. 2007. Lymphotoxin beta receptor signaling is required for inflammatory lymphangiogenesis in the thyroid. *Proc. Natl. Acad. Sci. USA* 104: 5026–5031.
 38. Thauinat, O., D. Kerjaschki, and A. Nicoletti. 2006. Is defective lymphatic drainage a trigger for lymphoid neogenesis? *Trends Immunol.* 27: 441–445.
 39. Cantaert, T., J. Kolln, T. Timmer, T. C. van der Pouw Kraan, B. Vandooren, R. M. Thurlings, J. D. Cañete, A. I. Catrina, T. Out, C. L. Verweij, et al. 2008. B lymphocyte autoimmunity in rheumatoid synovitis is independent of ectopic lymphoid neogenesis. *J. Immunol.* 181: 785–794.
 40. Motallebzadeh, R., E. M. Bolton, and G. J. Pettigrew. 2008. Lymphoid tissue formation in allografts: innocent until proven guilty. *Transplantation* 85: 309–311.
 41. Thurlings, R. M., C. A. Wijbrandts, R. E. Mebius, T. Cantaert, H. J. Dinant, T. C. van der Pouw-Kraan, C. L. Verweij, D. Baeten, and P. P. Tak. 2008. Synovial lymphoid neogenesis does not define a specific clinical rheumatoid arthritis phenotype. *Arthritis Rheum.* 58: 1582–1589.
 42. Di Carlo, E., T. D'Antuono, S. Contento, M. Di Nicola, E. Ballone, and C. Sorrentino. 2007. Quilty effect has the features of lymphoid neogenesis and shares CXCL13-CXCR5 pathway with recurrent acute cardiac rejections. *Am. J. Transplant.* 7: 201–210.
 43. Katakai, T., T. Nomura, H. Gonda, M. Sugai, Y. Agata, A. Nishio, T. Masuda, S. Sakaguchi, and A. Shimizu. 2006. Spontaneous large-scale lymphoid neogenesis and balanced autoimmunity versus tolerance in the stomach of H+K⁺-ATPase-reactive TCR transgenic mouse. *J. Immunol.* 177: 7858–7867.
 44. Fillatreau, S., D. Gray, and S. M. Anderton. 2008. Not always the bad guys: B cells as regulators of autoimmune pathology. *Nat. Rev. Immunol.* 8: 391–397.
 45. Thauinat, O., E. Morelon, and T. DeFrance. 2010. Am^B-valent: anti-CD20 antibodies unravel the dual role of B cells in immunopathogenesis. *Blood* E-published ahead of print.